Science Advances
AAAS

Supplementary Materials for

Photocatalytic production of ethylene and propionic acid from plastic waste by titania-supported atomically dispersed Pd species

Shuai Zhang *et al.*

Corresponding author: Jingrun Ran, jingrun.ran@adelaide.edu.au; Shi-Zhang Qiao, s.qiao@adelaide.edu.au

Sci. Adv. **9**, eadk2407 (2023)
DOI: 10.1126/sciadv.adk2407

This PDF file includes:

Figs. S1 to S18
Tables S1 to S10
References

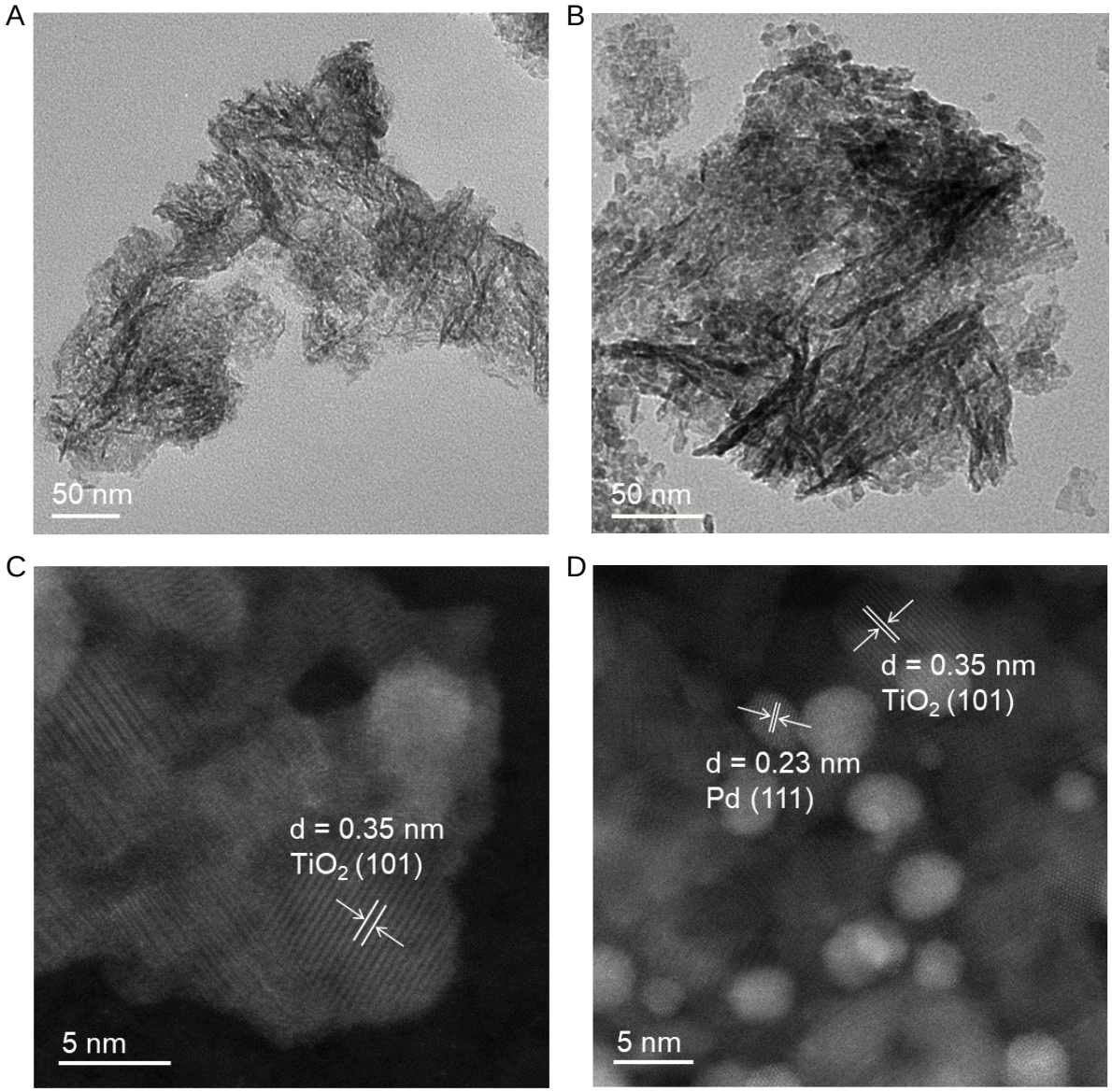

Fig. S1. Morphology characterizations. High-resolution transmission electron microscopy (HRTEM) images of (**A**) TiO_2 and (**B**) Pd_n-TiO_2. High-angle annular dark-field scanning transmission electron microscopy (HAADF-STEM) images of (**C**) TiO_2 and (**D**) Pd_n-TiO_2.

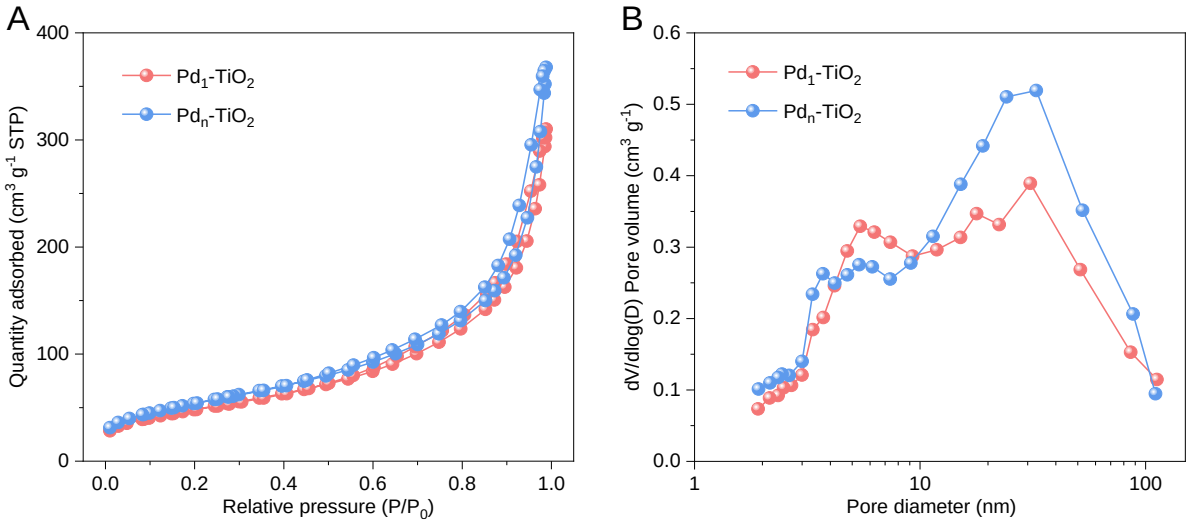

Fig. S2. Nitrogen (N_2) adsorption analysis. (**A**) N_2 adsorption-desorption isotherms and (**B**) the corresponding pore size distributions for Pd_1-TiO_2 and Pd_n-TiO_2.

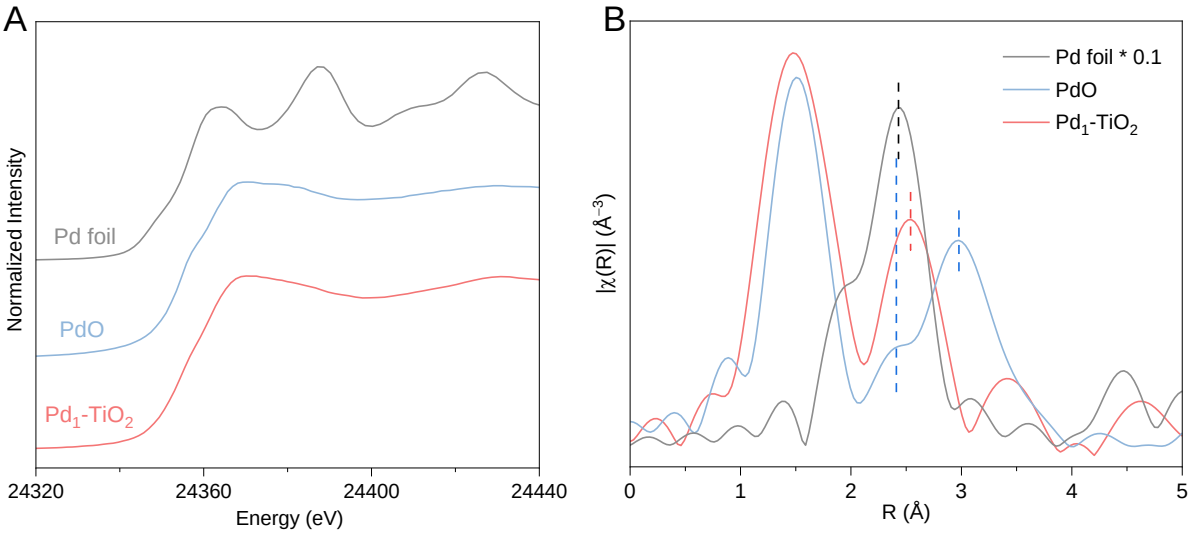

Fig. S3. Atomic structure characterizations. (**A**) Pd K-edge X-ray absorption near edge structure spectra and (**B**) Fourier-transformed k^2-weighted extended X-ray absorption fine structure (EXAFS) spectra for Pd foil, PdO and Pd_1-TiO_2.

fig. S3B exhibits a shoulder for PdO reference, which is closely aligned with the Pd foil. The EXAFS fitting in table S2 indicates that the shoulder peak can be assigned to Pd-Pd coordination.

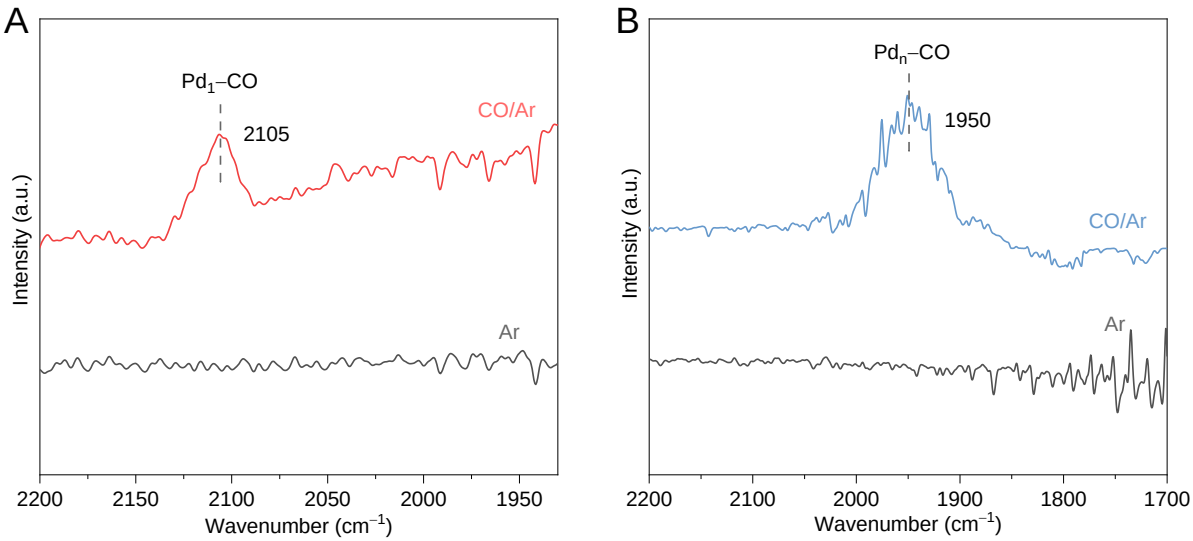

Fig. S4. CO adsorption diffuse reflectance infrared Fourier transform spectroscopy (DRIFTS) spectra. (**A**) Pd_1-TiO_2 and (**B**) Pd_n-TiO_2.

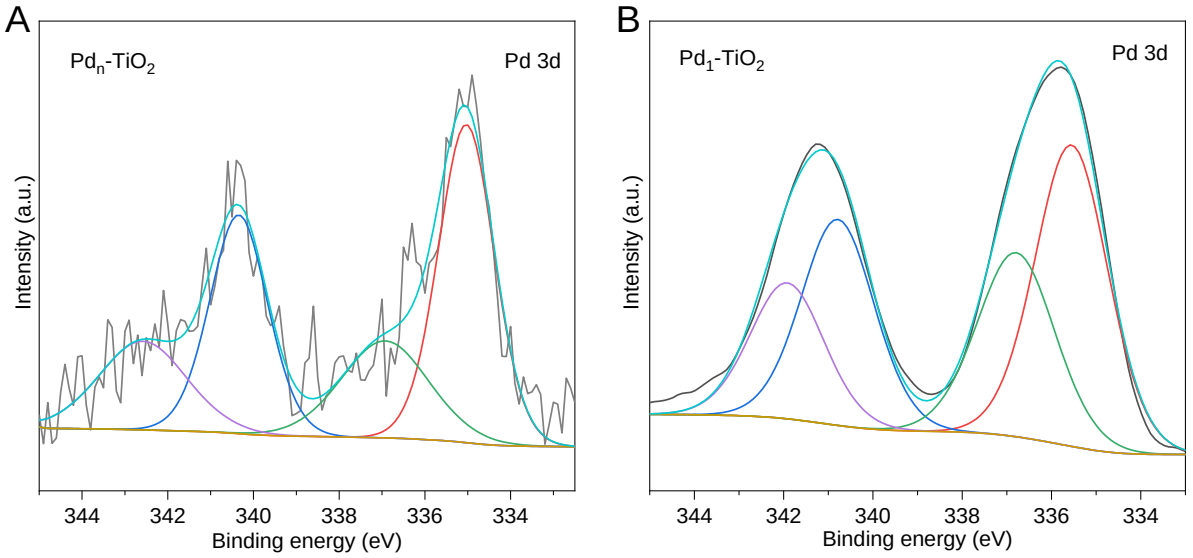

Fig. S5. Pd 3d X-ray photoelectron spectroscopy (XPS) spectra. (**A**) Pd_n-TiO_2 and (**B**) Pd_1-TiO_2.

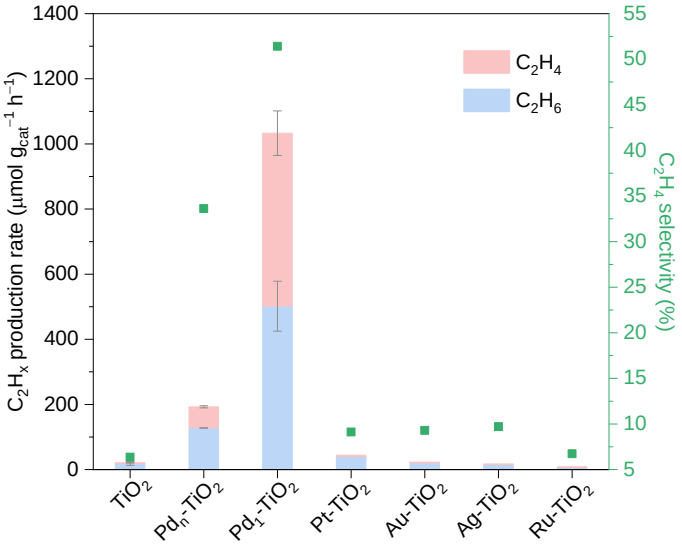

Fig. S6. C_2 hydrocarbon (C_2H_x) production for bare TiO_2 and a series of TiO_2 catalysts modified with metal species following 3 h of photoreaction.

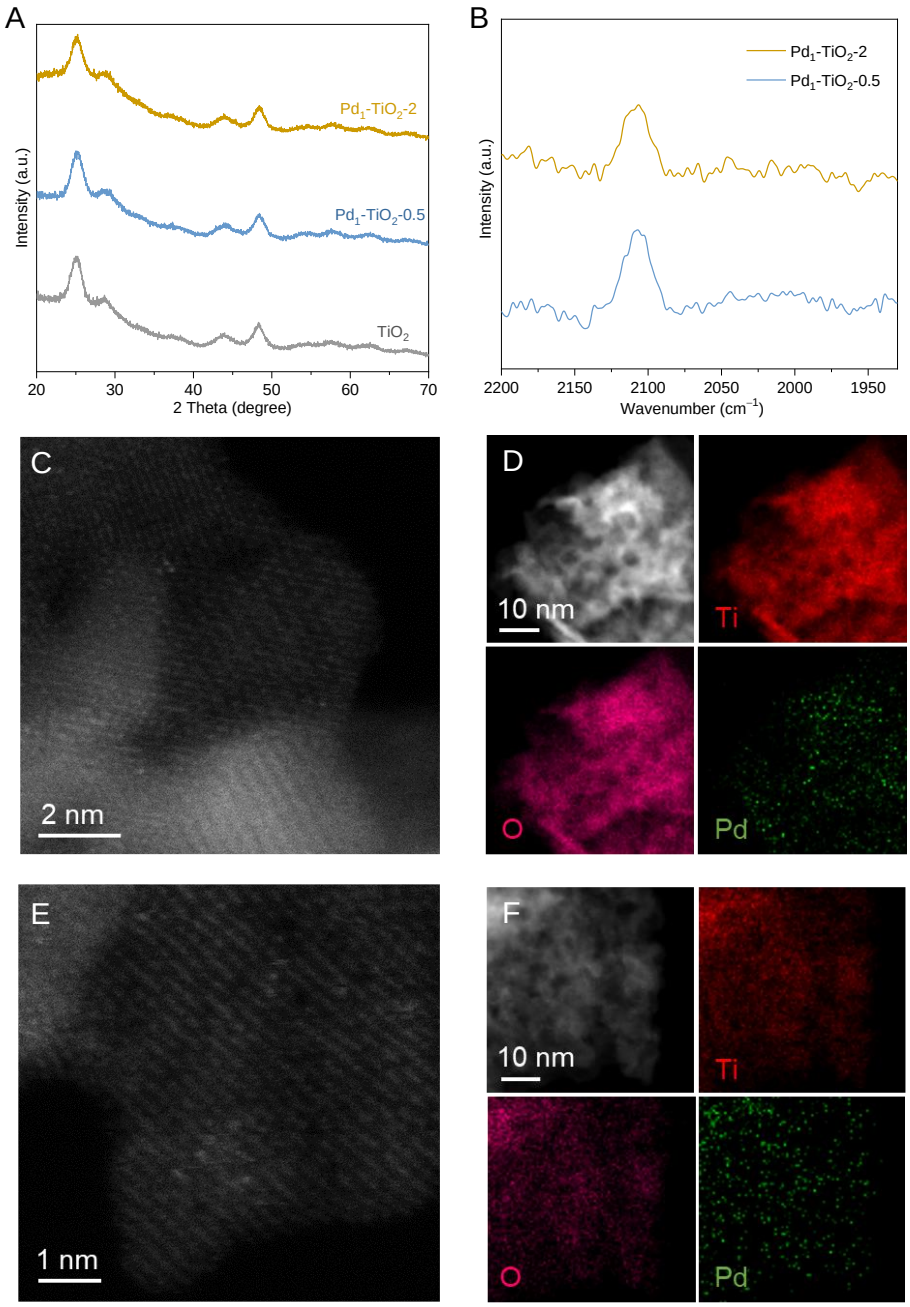

Fig. S7. Characterization of Pd_1-TiO_2-0.5 and Pd_1-TiO_2-2. (**A**) X-ray diffraction (XRD) patterns for TiO_2, Pd_1-TiO_2-0.5 and Pd_1-TiO_2-2. (**B**) CO adsorption DRIFTS spectra of Pd_1-TiO_2-0.5 and Pd_1-TiO_2-2. (**C**) HAADF-STEM image and (**D**) Energy dispersive spectroscopy **(**EDS) mapping of Pd_1-TiO_2-0.5. (**E**) HAADF-STEM image and (**F**) EDS mapping of Pd_1-TiO_2-2.

The XRD patterns for Pd_1-TiO_2-0.5 and Pd_1-TiO_2-2 exhibit the diffraction peaks for anatase TiO_2 without Pd-related features (fig. S7A). For the CO adsorption, a typical band for linearly adsorbed CO is observed at 2050~2150 cm^{-1} (fig. S7B). The result indicates the atomic dispersion of Pd species on Pd_1-TiO_2-0.5 and Pd_1-TiO_2-2. This is also confirmed by the HAADF-STEM images (fig. S7, C to F), in which atomic Pd sites are dispersed on TiO_2 nanosheets.

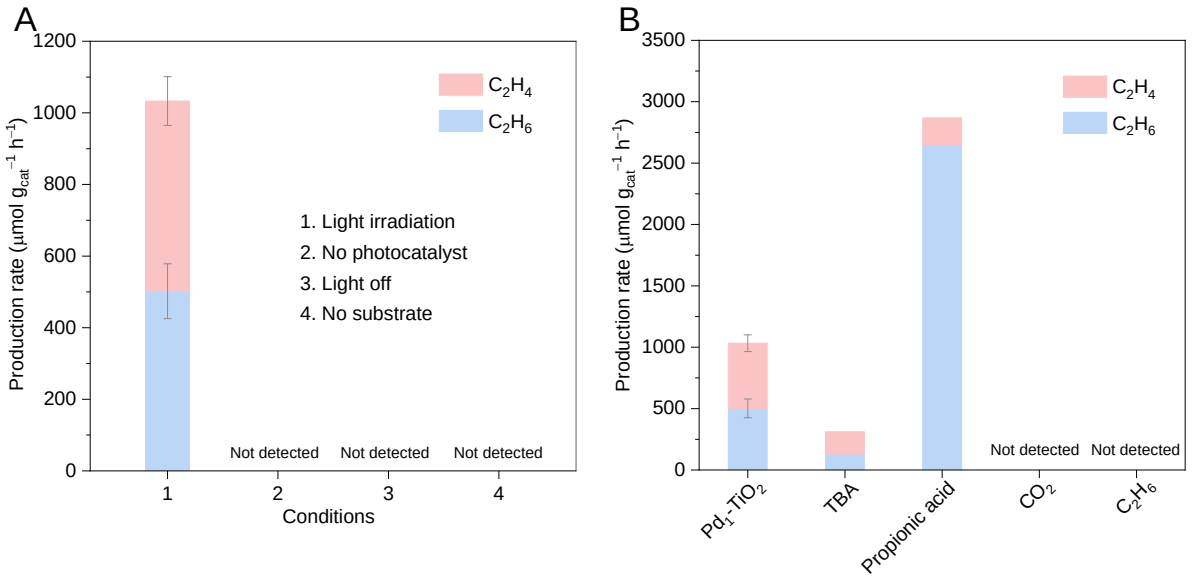

Fig. S8. Control experiments. (**A**) Summary of experimental control conditions for photocatalytic substrate oxidation over Pd_1-TiO_2. (**B**) Photocatalytic generation of C_2 hydrocarbons on Pd_1-TiO_2 by converting succinic acid in the presence of tert-butanol or by using different starting substrates such as propionic acid, CO_2, and ethane (C_2H_6). C_2 hydrocarbon production is expressed per mass of photocatalyst.

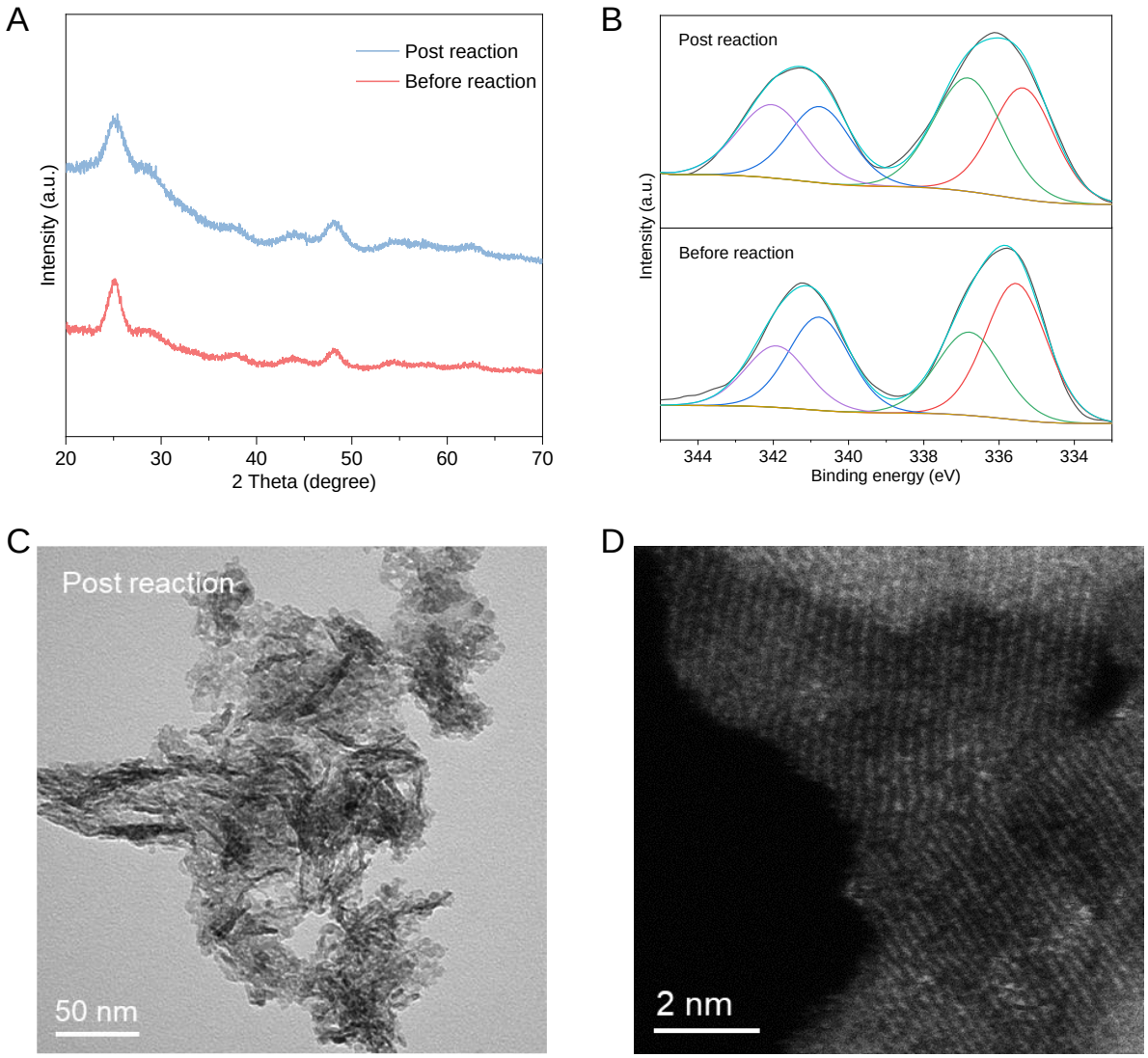

Fig. S9. Material characterization of the post-reaction sample. (**A**) XRD pattern, (**B**) Pd 3d XPS spectra, (**C**) HRTEM and (**D**) HAADF-STEM images of Pd_1-TiO_2.

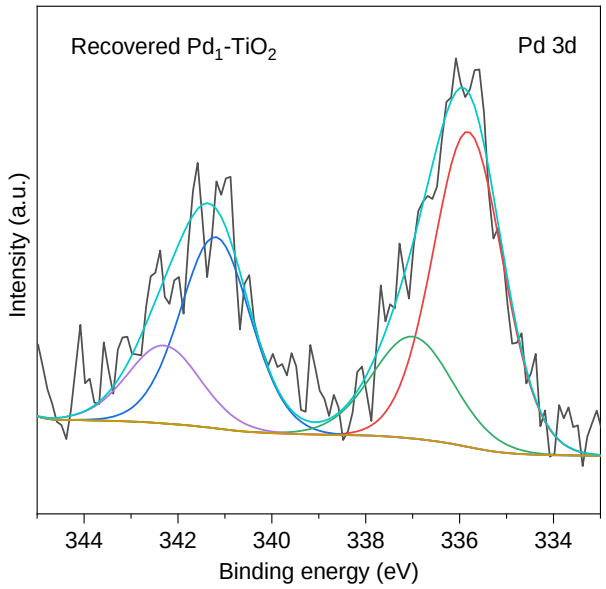

Fig. S10. Pd 3d XPS spectrum of the recovered Pd_1-TiO_2 after illumination and vacuum drying.

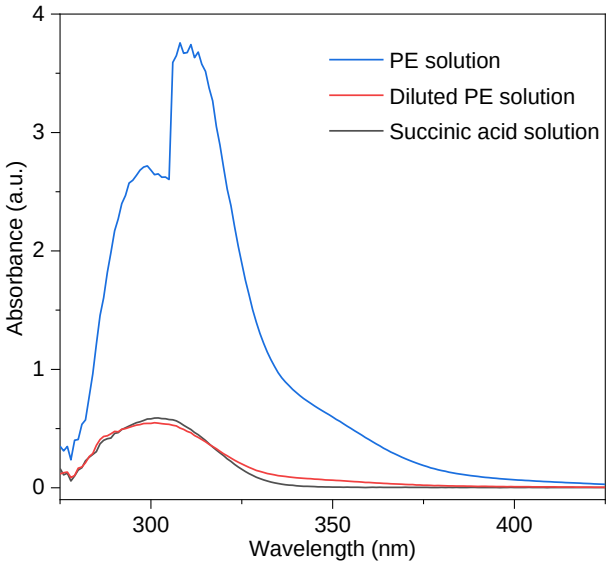

Fig. S11. UV-vis absorption spectra of succinic acid substrate solution, diluted PE decomposition solution, and pure polyethylene (PE) decomposition solution.

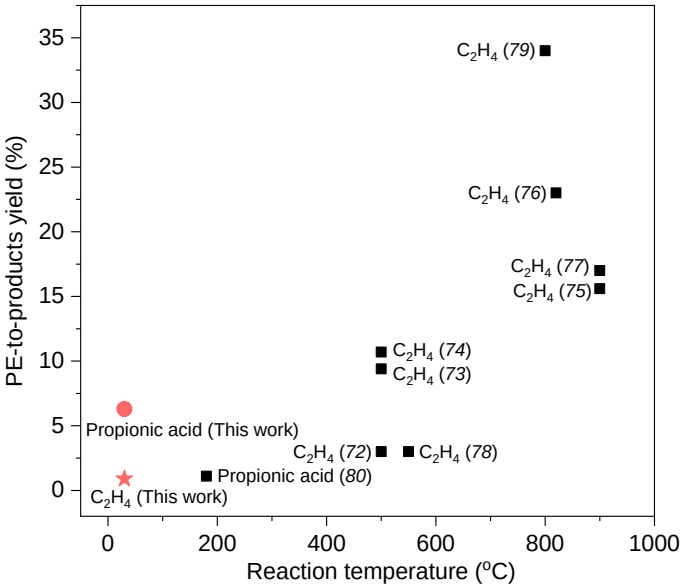

Fig. S12. The PE-to-single product (C_2H_4 or propionic acid) conversion achieved via oxidation-photocatalysis and high-temperature thermocatalysis. Catalysts and reaction processes for reported data are as follows: Y zeolite pyrolysis (*72*), HZSM-5 pyrolysis (*73*), $Al(OH)_3$ pyrolysis (*74*), HZSM-11 pyrolysis (*75*), blend with naphtha for pyrolysis-steam cracking (*76*), biomass co-gasification (*77*), HZSM-5 pyrolysis-steam cracking (*78*), non-catalysis pyrolysis (*79*) and microwave assisted chemical oxidation (*80*).

Selected reports on thermocatalytic conversion of plastic waste into C_2H_4/propionic acid were added in fig. S12 for comparison with our low-temperature oxidation-photocatalysis. Pyrolysis of PE waste requires high temperatures (>450 °C) and yields the major products of C_5-C_{20+} hydrocarbons as well as C_1-C_4 hydrocarbons. High temperatures, fluidized bed systems and catalysts were explored to improve C_2H_4 recovery. Gasification of PE is conducted at >600°C to convert carbon-based feedstocks into primarily gaseous products. Steam gasification of PE has been reported to produce C_2H_4 at relatively high temperature (900 °C). Two step processes, including gasification-FT synthesis, pyrolysis-steam cracking, can achieve a high yield of light olefins. Propionic acid has been rarely reported to be generated from PE waste. Microwave-assisted chemical oxidation of PE yields a series of carboxylic acids including a portion of propionic acid.

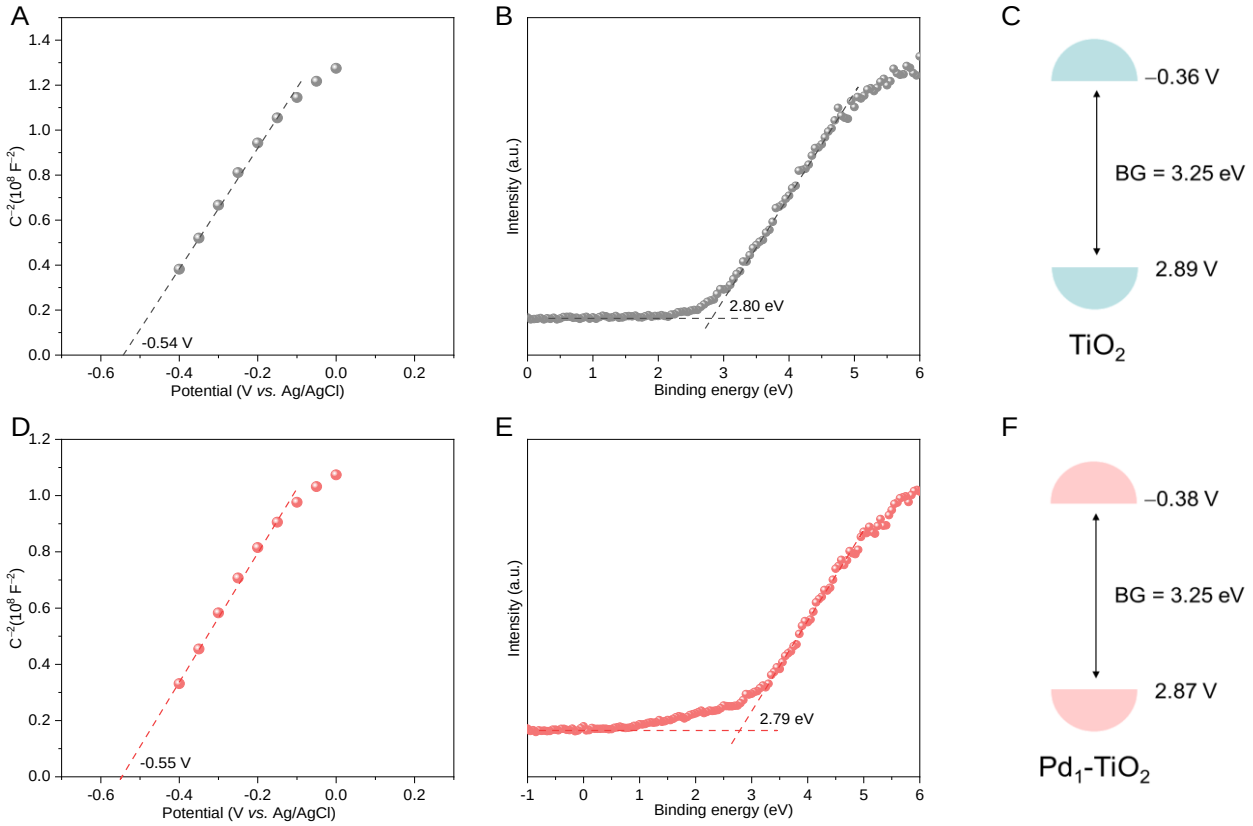

Fig. S13. Energy band structure characterizations. (**A**) Mott-Schottky (MS) plot, (**B**) XPS valence band (VB) spectrum and (**C**) schematic for energy band structure for TiO_2. (**D**) MS plot, (**E**) XPS VB spectrum and (**F**) schematic for energy band structure for Pd_1-TiO_2.

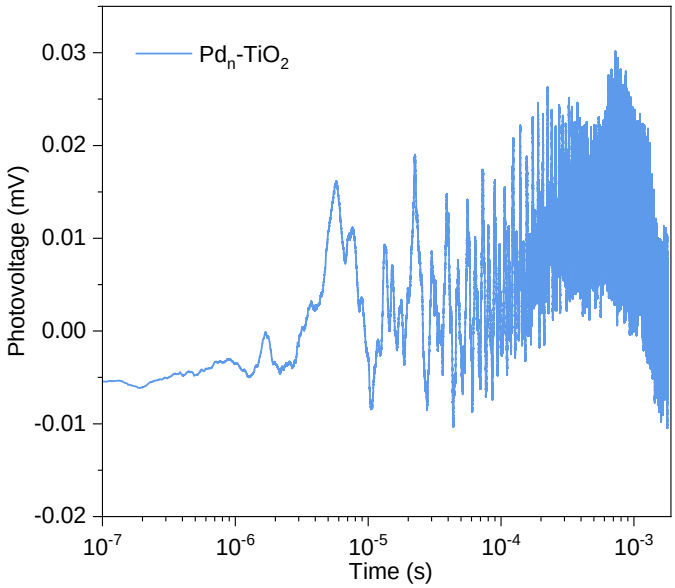

Fig. S14. Transient surface photovoltage spectrum for Pd_n-TiO_2.

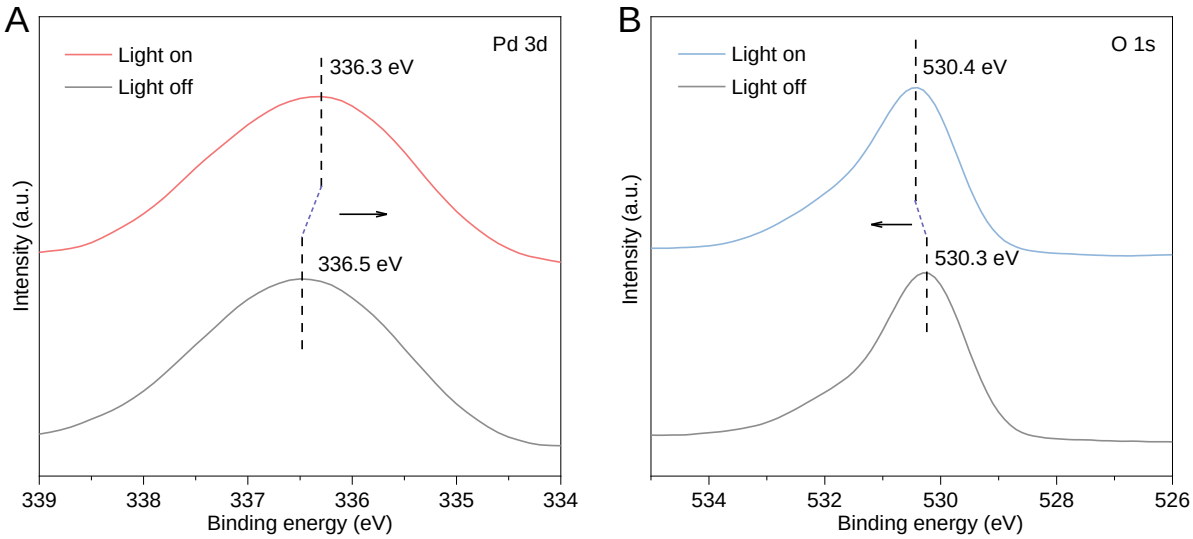

Fig. S15. XPS spectra. (**A**) An enlarged view of Pd 3d XPS spectrum and (**B**) O 1s XPS spectrum for Pd_1-TiO_2 in dark and under illumination.

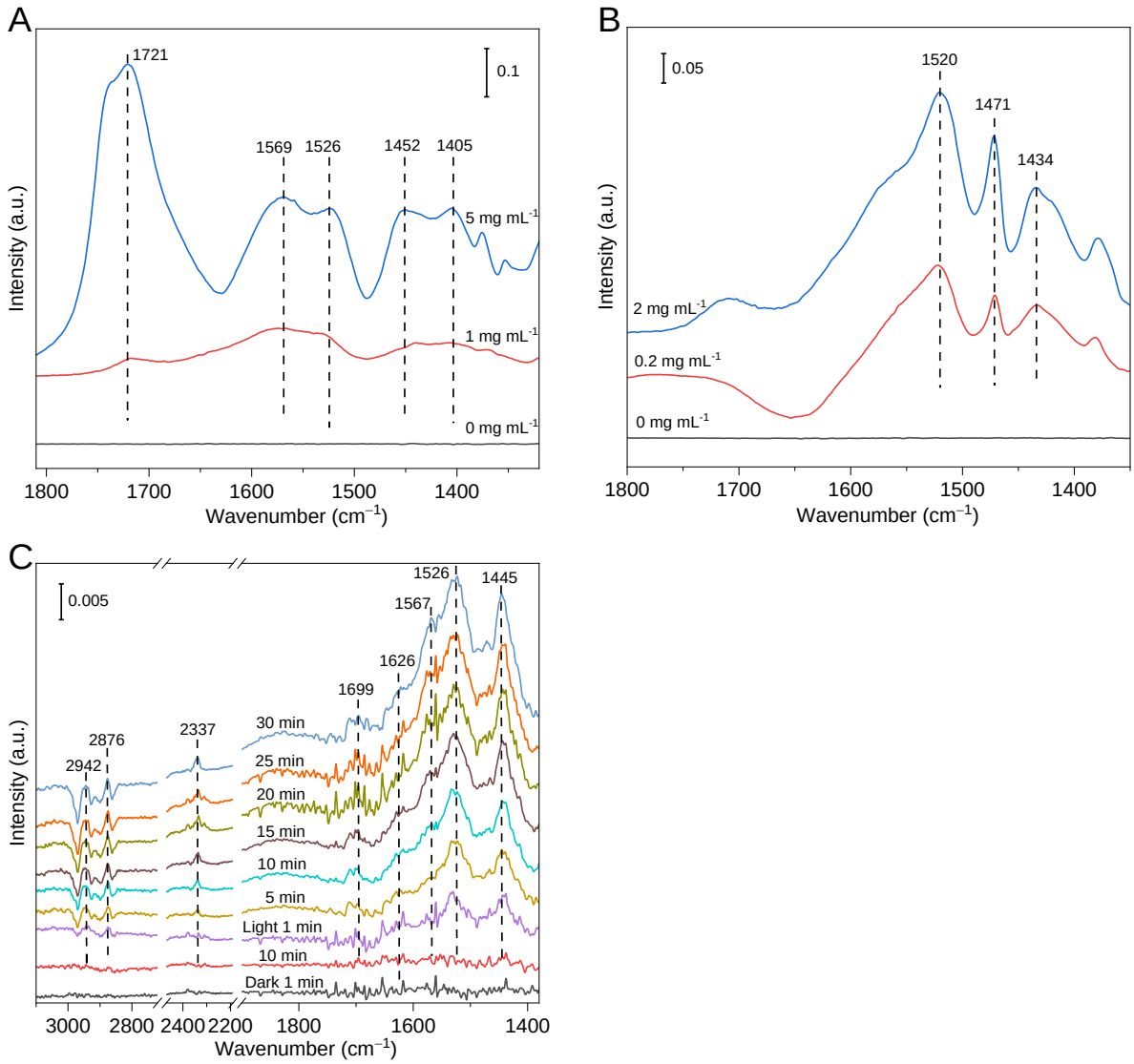

Fig. S16. DRIFTS characterizations. DRIFTS spectra for different concentrations of (**A**) succinic acid and (**B**) propionic acid on Pd_1-TiO_2 in the dark. (**C**) In situ DRIFTS spectra for the substrate conversion on Pd_n-TiO_2.

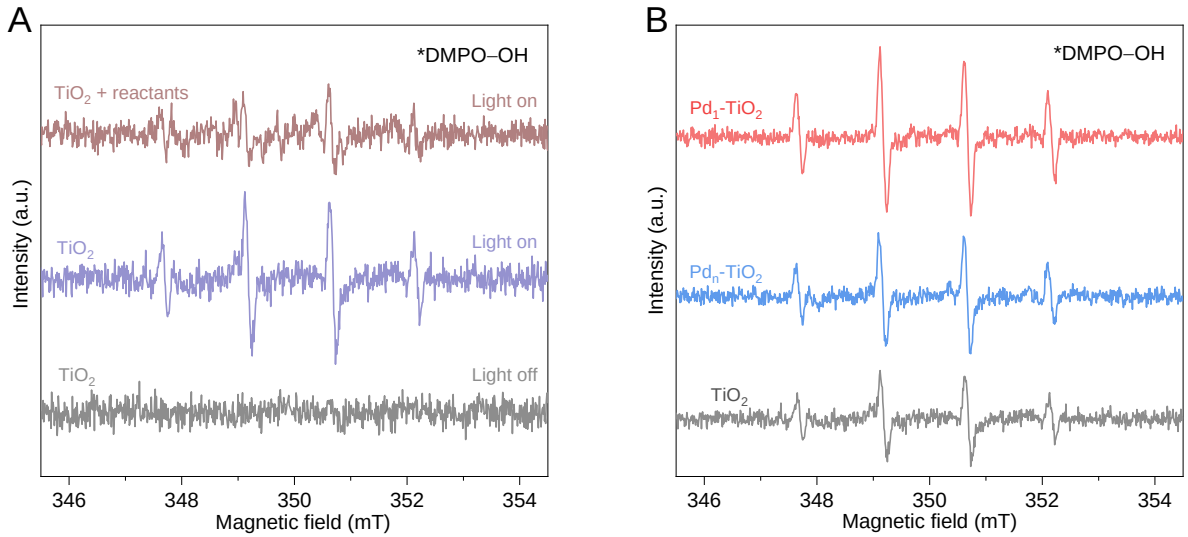

Fig. S17. Electron paramagnetic resonance (EPR) charcaterizations. (**A**) In situ EPR spectra for TiO_2 with and without reaction substrates under light irradiation. (**B**) In situ EPR spectra for hydroxyl radical (·OH) detection over TiO_2, Pd_1-TiO_2 and Pd_n-TiO_2 without reaction substrates under light irradiation.

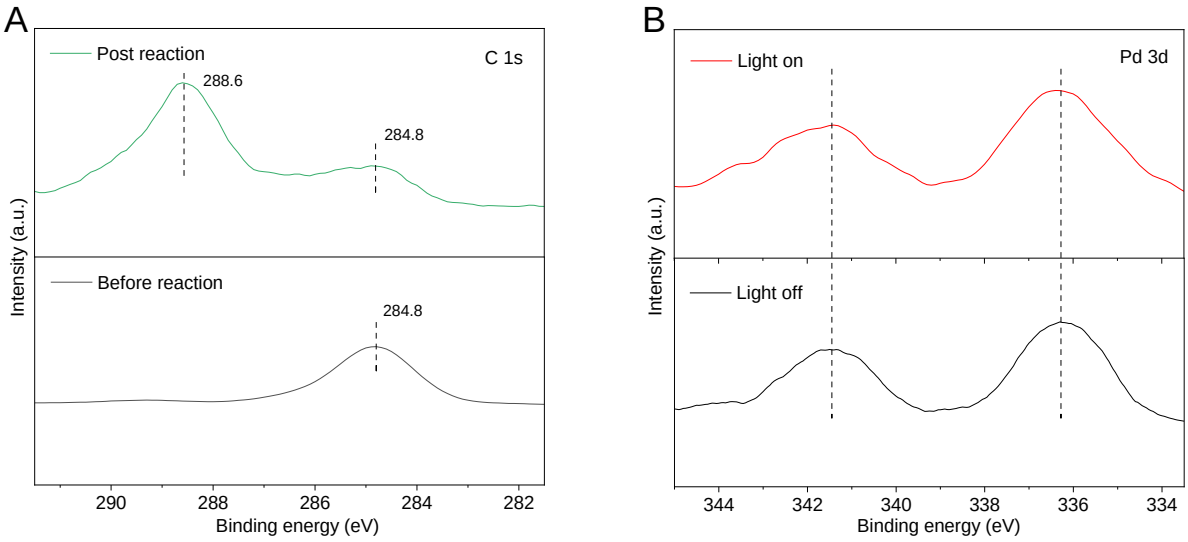

Fig. S18. XPS spectra. (**A**) C 1s XPS spectra for Pd_1-TiO_2 before and after photoreaction. (**B**) In situ high-resolution Pd 3d XPS spectra for Pd_1-TiO_2 with the substrate and illumination.

Table S1. Physicochemical properties of Pd_1-TiO_2 and Pd_n-TiO_2.

Sample	Pd (wt.%)	Surface area (m^2 g^{-1})	Average pore size (nm)
Pd_1-TiO_2	0.64	176	9.9
Pd_n-TiO_2	0.70	199	10.7

Table S2. EXAFS fitting results for Pd_1-TiO_2 and PdO. CN is the coordination number, R distance between absorber and backscatter atoms and σ^2 Debye-Waller factor.

Sample	Shell	CN	R (Å)	σ^2(Å^2)
	Pd-O	2.9	2.05	0.006
Pd_1-TiO_2	Pd-Pd	3.0	2.75	0.011
	Pd-Ti	2.1	2.94	0.012
	Pd-O	1.8	2.02	0.003
PdO	Pd-Pd (shoulder)	1.1	2.92	0.004
	Pd-Pd	0.8	2.96	0.002

Table S3. Photocatalytic generation of C_2 hydrocarbons from succinic acid substrate at different pH values over Pd_1-TiO_2.

pH value	C_2H_4 production (μmol g_{cat}^{-1} h^{-1})	C_2H_6 production (μmol g_{cat}^{-1} h^{-1})
1	192.51	124.04
4	531.16	501.84
7	4.59	6.85
10	N/A	N/A

Table S4. Photocatalytic generation of C_2 hydrocarbons from succinic acid substrate over Pd_1-TiO_2 at 30ºC, 50ºC and 70ºC.

Temperature (ºC)	C_2H_4 production ($\mu mol\ g_{cat}^{-1}\ h^{-1}$)	C_2H_6 production ($\mu mol\ g_{cat}^{-1}\ h^{-1}$)
30	531.16	501.84
50	498.41	440.06
70	444.88	417.24

Table S5. Inductively coupled plasma optical emission spectrometry. The Pd loading in Pd_1-TiO_2 before and after photoreactions.

Conditions	Pd (wt.%)
Before reaction	0.64
Post reaction	0.63

Table S6. The amounts of H_2 and CO_2 evolved. Photocatalytic substrate conversion over TiO_2, Pd_1-TiO_2 and Pd_n-TiO_2 following 3 h light irradiation.

Sample	Reaction time (h)	H_2 yield (mmol)	CO_2 yield (mmol)
TiO_2	3	N/A	0.11
Pd_1-TiO_2	3	0.04	0.49
Pd_n-TiO_2	3	0.03	0.38

Table S7. Solar-driven upcycling of plastic waste for selected state-of-the-art catalysts.

Catalyst	Substrate(s)	Light source(s)	Catalyst mass (mg or cm^{-2})	Time (h)	Gaseous product production (μmol g_{cat}^{-1} h^{-1} or μmol cm^{-2} h^{-1})	Liquid phase product yield (μmol or %)	Reference
Pd_1-TiO_2	10 mg mL^{-1} succinic acid in 0.1 M HNO_3	365 nm LED	10	3	C_2H_4: 531.16, C_2H_6: 501.84 H_2, CO_2	Propionic acid: 493.3	This work
Pd_1-TiO_2	2 mg mL^{-1} PE solution	365 nm LED	30	3	C_2H_4: 23.28, C_2H_6: 32.73 H_2, CO_2	Propionic acid: 23.9	This work
P25|Pt	10 mg mL^{-1} succinic acid in 0.1 M HNO_3	AM 1.5G	4	24	C_2H_6: 56.3, H_2, CO_2	Propionic acid: 92.6	(*7*)
$^{NCN}CN_x$|Pt	10 mg mL^{-1} succinic acid in 0.1 M HNO_3	AM 1.5G	4	24	C_2H_4: 1.3, C_2H_6: 7.2 H_2, CO_2	Propionic acid: 17	(*7*)
P25|Pt	2.7 mg mL^{-1} PE solution	AM 1.5G	4	96	C_2H_4: 0.21, C_2H_6: 2.6 H_2, CO_2	N/A	(*7*)
MoS_2/CdS	25 mg mL^{-1} PE solution	AM 1.5G	100	5	CH_4: 196.2, H_2: 900	Formic acid: 9100	(*45*)
d-$NiPS_3$/CdS	10 mg mL^{-1} Polylactic acid (PLA) in 2 M KOH	300 W Xe lamp	1	3	H_2: 39760	Pyruvate: 39.03 (9 h), carbonate	(*66*)
d-$NiPS_3$/CdS	50 mg mL^{-1} polyethylene glycol (PET) in 2 M KOH	300 W Xe lamp	1	3	H_2: 31380	Glycolate: 16.42 (9 h) carbonate	(*66*)
CN_x|Ni_2P	50 mg mL^{-1} PLA in 1 M KOH	AM 1.5G	3.2	20	H_2: 47	Acetate: 0.1 (120 h)	(*81*)
CN_x|Ni_2P	25 mg mL^{-1} PET in 1 M KOH	AM 1.5G	3.2	20	H_2: 26	Glyoxal: 9.3 (120 h)	(*81*)
Nb_2O_5	150 mg PE in 50 mL water	300 W Xe lamp, AM 1.5G filter	50	40	CO_2	Acetic acid: 1.58	(*46*)
Co-Ga_2O_3	100 mg PE in 100 mL water	300 W Xe lamp, AM 1.5G filter	50	24	H_2: 692, CO: 177.8 CO_2	N/A	(*82*)
Fluorenone	20.8 mg polystyrene (PS) in 2 mL ethyl acetate	450 nm LED	40 μmol	48	CO, CO_2	Benzoic acid: 38%	(*14*)
Triflic acid	104 mg PS in 2 mL of benzene and acetonitrile	405 nm LED	5 mol%	15	N/A	Formic acid: 72%	(*83*)
ZnO/UiO66-NH_2	1 g Polyvinyl chloride in 50 mL water	300 W Xe lamp	100	35	H_2	Acetic acid: 9.2%	(*84*)
M. b-CDPCN	50 mg mL^{-1} PLA and CO_2	395 nm LED	N/A	576	CH_4: 12.57	N/A	(*85*)
C_3N_4	500 mg PS in acetonitrile	300 W Xe lamp, 150ºC	200	160	CO_2	Benzoic acid: 2184	(*86*)
Co SSCs	500 mg PET in ethylene glycol	simulated sunlight, 180ºC	15	3	N/A	bis(2-hydroxyethyl) terephthalate: 82.6%	(*87*)
$Cu_{30}Pd_{70}$|Perovskite|Pt	50 mg mL^{-1} PET in 1 M KOH	AM 1.5G	Electrode : 1.5 cm^2	10	H_2: 77.6 μmol cm^{-2} h^{-1}	Glycolic acid: 82	(*88*)
nanoNi-P	40 mg mL^{-1} PET in 2 M KOH	AM 1.5G	Electrode : 1.0 cm^2	1	H_2: 3.1 μmol cm^{-2} h^{-1}	Formic acid: 244.6	(*89*)

Generation of valuable major products are included.

Selected reports on photocatalytic treatment of plastic waste are added in table S7, including (1) plastic photoreforming, (2) chemical oxidation-decarboxylation, (3) photocatalytic degradation-CO_2 reduction as well as (4) homogeneous catalytic C-C/C-H activation. (1) Photoreforming of plastic waste involves: i) decomposition of plastic waste into monomers; ii) photocatalytic hydrogen evolution coupled with oxidation of monomers into oxygenates. Advanced CdS-based photocatalysts exhibit excellent performance with a hydrogen evolution of ~40 mmol g_{cat}^{-1} h^{-1}. However, the oxidation reaction still suffers from low selectivity towards a single high-value product and overoxidation to CO_2. (2) The reported PE upcycling via chemical oxidation-decarboxylation represents an emerging strategy to simultaneously generate valuable light olefins and single carboxylic acid with high selectivity. Side products generated from chemical oxidation may compete with the main reaction and reduce its activity. (3) One-pot photodegradation coupled with CO_2 reduction can decompose plastic waste with a conversion of nearly 100%, while enabling CO_2 photoreduction. The two-step process can be carried out under mild conditions, but generally requires tens of hours of irradiation to achieve complete decomposition of plastic waste. (4) Upcycling of aromatic polymers has been reported using homogeneous photocatalysts and O_2. Photo-driven hydrogen atom transfer followed by C-C cleavage enable the direct conversion of plastic waste into aromatic oxygenates with high yields (> 40%). Organic solvents are employed to dissolve plastics but make the reaction system complex and toxic.

Additionally, other solar-driven chemical recycling methods are also reported in table S7, including photo-biocatalysis, photothermal catalysis and photoelectrocatalysis. The biotic-abiotic hybrid methanation of microplastics exhibits excellent stability (up to 4 months) and high selectivity to CH_4, but the CH_4 yield needs to be improved. Photothermal catalysis can utilize sunlight to heat up the reaction system and boost plastic conversion, but it also aggravates overoxidation. The photothermal effect is a promising strategy that can be applied to thermocatalytic plastic conversions. The current studies on photoelectrocatalysis focus on the reforming of plastics into H_2 and chemicals. Compared to photoreforming, plastic monomer oxidation on the photoelectrode surface can be regulated to achieve high selectivity (up to 90%) to a single valuable oxygenate.

Table S8. Quantification of components of PE decomposition solution following pretreatment.

Conditions	Concentration (5-fold diluted) (mg mL^{-1})			
	Succinic acid	Acetic acid	Glutaric acid	Adipic acid
160°C 8 h	1.98	0.30	0.89	0.01

Table S9. C_2 hydrocarbon evolution on Pd_1-TiO_2 in PE solutions with ultrapure water, seawater, rainwater, and simulated nitric acid wastewater as solvents. C_2 hydrocarbon production is expressed per mass of photocatalyst.

Sample	Solvent	C_2H_4 production (μmol g_{cat}^{-1} h^{-1})	C_2H_6 production (μmol g_{cat}^{-1} h^{-1})
Pd_1-TiO_2	Ultrapure water	23.28	32.73
	Seawater	13.65	19.16
	Rainwater	15.42	18.80
	Simulated wastewater	17.85	20.20

Table S10. Pd $3d_{5/2}$ XPS of Pd_1-TiO_2 in dark and under illumination.

Samples	Peak	Positions (eV)	FWHM	Percentage
In dark	Pd^0	336.20	2.00	68%
	Pd^{2+}	337.42	1.90	32%
Light irradiation	Pd^0	336.18	2.00	73%
	Pd^{2+}	337.40	1.90	27%

REFERENCES AND NOTES

1. T. Uekert, C. M. Pichler, T. Schubert, E. Reisner, Solar-driven reforming of solid waste for a sustainable future. *Nat. Sustain.* **4**, 383–391 (2021).

2. R. Geyer, J. R. Jambeck, K. L. Law, Production, use, and fate of all plastics ever made. *Sci. Adv.* **3**, e1700782 (2017).

3. X. Jia, C. Qin, T. Friedberger, Z. Guan, Z. Huang, Efficient and selective degradation of polyethylenes into liquid fuels and waxes under mild conditions. *Sci. Adv.* **2**, e1501591. (2016).

4. F. Zhang, M. Zeng, R. D. Yappert, J. Sun, Y.-H. Lee, A. M. LaPointe, B. Peters, M. M. Abu-Omar, S. L. Scott, Polyethylene upcycling to long-chain alkylaromatics by tandem hydrogenolysis/aromatization. *Science* **370**, 437–441 (2020).

5. G. Lopez, M. Artetxe, M. Amutio, J. Bilbao, M. Olazar, Thermochemical routes for the valorization of waste polyolefinic plastics to produce fuels and chemicals. A review. *Renew. Sustain. Energy Rev.* **73**, 346–368 (2017).

6. K. Hu, P. Zhou, Y. Yang, T. Hall, G. Nie, Y. Yao, X. Duan, S. Wang, Degradation of microplastics by a thermal fenton reaction. *ACS EST Engg.* **2**, 110–120 (2022).

7. C. M. Pichler, S. Bhattacharjee, M. Rahaman, T. Uekert, E. Reisner, Conversion of polyethylene waste into gaseous hydrocarbons via integrated tandem chemical-photo/electrocatalytic processes. *ACS Catal.* **11**, 9159–9167 (2021).

8. H. Nishiyama, T. Yamada, M. Nakabayashi, Y. Maehara, M. Yamaguchi, Y. Kuromiya, Y. Nagatsuma, H. Tokudome, S. Akiyama, T. Watanabe, R. Narushima, S. Okunaka, N. Shibata, T. Takata, T. Hisatomi, K. Domen, Photocatalytic solar hydrogen production from water on a 100-m^2 scale. *Nature* **598**, 304–307 (2021).

9. J. Xie, R. Jin, A. Li, Y. Bi, Q. Ruan, Y. Deng, Y. Zhang, S. Yao, G. Sankar, D. Ma, J. Tang, Highly selective oxidation of methane to methanol at ambient conditions by titanium dioxide-supported iron species. *Nat. Catal.* **1**, 889–896 (2018).

10. S. Zhang, Y. Zhao, R. Shi, C. Zhou, G. I. N. Waterhouse, Z. Wang, Y. Weng, T. Zhang, Sub-3 nm ultrafine Cu_2O for visible light driven nitrogen fixation. *Angew. Chem. Int. Ed.* **60**, 2554–2560 (2021).

11. S. Nitopi, E. Bertheussen, S. B. Scott, X. Liu, A. K. Engstfeld, S. Horch, B. Seger, I. E. L. Stephens, K. Chan, C. Hahn, J. K. Nørskov, T. F. Jaramillo, I. Chorkendorff, Progress and perspectives of electrochemical CO_2 reduction on copper in aqueous electrolyte. *Chem. Rev.* **119**, 7610–7672 (2019).

12. L. Li, R.-B. Lin, R. Krishna, H. Li, S. Xiang, H. Wu, J. Li, W. Zhou, B. Chen, Ethane/ethylene separation in a metal-organic framework with iron-peroxo sites. *Science* **362**, 443–446 (2018).

13. G. Lopez, M. Artetxe, M. Amutio, J. Alvarez, J. Bilbao, M. Olazar. Recent advances in the gasification of waste plastics. A critical overview. *Renew. Sustain. Energy Rev.* **82**, 576–596 (2018).

14. T. Li, A. Vijeta, C. Casadevall, A. S. Gentleman, T. Euser, E. Reisner. Bridging plastic recycling and organic catalysis: Photocatalytic deconstruction of polystyrene via a C-H oxidation pathway. *ACS Catal.* **12**, 8155–8163 (2022).

15. Z. Huang, Z. Zhao, C. Zhang, J. Lu, H. Liu, N. Luo, J. Zhang, F. Wang, Enhanced photocatalytic alkane production from fatty acid decarboxylation via inhibition of radical oligomerization. *Nat. Catal.* **3**, 170–178 (2020).

16. B. Kraeutler, A. J. Bard, Heterogeneous photocatalytic decomposition of saturated carboxylic acids on titanium dioxide powder. Decarboxylative route to alkanes. *J. Am. Chem. Soc.* **100**, 5985–5992 (1978).

17. J. D. Griffin, M. A. Zeller, D. A. Nicewicz, Hydrodecarboxylation of carboxylic and malonic acid derivatives via organic photoredox catalysis: Substrate scope and mechanistic insight. *J. Am. Chem. Soc.* **137**, 11340–11348 (2015).

18. I. Eş, A. M. Khaneghah, S. M. B. Hashemi, M. Koubaa, Current advances in biological production of propionic acid. *Biotechnol. Lett.* **39**, 635–645 (2017).

19. U.-R. Samel, W. Kohler, A. O. Gamer, U. Keuser, S.-T. Yang, Y. Jin, M. Lin, Z. Wang, J. H. Teles. Propionic acid and derivatives, in *Ullmann's Encyclopedia of Industrial Chemistry* (Wiley-VCH, 2018), pp. 1–20.

20. S. Ji, Y. Chen, X. Wang, Z. Zhang, D. Wang, Y. Li, Chemical synthesis of single atomic site catalysts. *Chem. Rev.* **120**, 11900–11955 (2020).

21. A. Wang, J. Li, T. Zhang, Heterogeneous single-atom catalysis. *Nat. Rev. Chem.* **2**, 65–81 (2018).

22. C. Gao, J. Low, R. Long, T. Kong, J. Zhu, Y. Xiong, Heterogeneous single-atom photocatalysts: Fundamentals and applications. *Chem. Rev.* **120**, 12175–12216 (2020).

23. B. Xia, Y. Zhang, J. Ran, M. Jaroniec, S.-Z. Qiao, Single-atom photocatalysts for emerging reactions. *ACS Cent. Sci.* **7**, 39–54 (2021).

24. R. Li, Z. Zhang, X. Liang, J. Shen, J. Wang, W. Sun, D. Wang, J. Jiang, Y. Li, Polystyrene waste thermochemical hydrogenation to ethylbenzene by a N-bridged Co, Ni dual-atom catalyst. *J. Am. Chem. Soc.* **145**, 16218–16227 (2023).

25. R. Li, D. Wang, Understanding the structure-performance relationship of active sites at atomic scale. *Nano Res.* **15**, 6888–6923 (2022).

26. X. Ge, P. Zhou, Q. Zhang, Z. Xia, S. Chen, P. Gao, Z. Zhang, L. Gu, S. Guo, Palladium single atoms on TiO_2 as a photocatalytic sensing platform for analyzing the organophosphorus pesticide chlorpyrifos. *Angew. Chem. Int. Ed.* **59**, 232–236 (2020).

27. W. Jiang, J. Low, K. Mao, D. Duan, S. Chen, W. Liu, C.-W. Pao, J. Ma, S. Sang, C. Shu, X. Zhan, Z. Qi, H. Zhang, Z. Liu, X. Wu, R. Long, L. Song, Y. Xiong, Pd-modified ZnO-Au enabling alkoxy intermediates formation and dehydrogenation for photocatalytic conversion of methane to ethylene. *J. Am. Chem. Soc.* **143**, 269–278 (2021).

28. Y. Guo, Y. Huang, B. Zeng, B. Han, M. Akri, M. Shi, Y. Zhao, Q. Li, Y. Su, L. Li, Q. Jiang, Y.-T. Cui, L. Li, R. Li, B. Qiao, T. Zhang, Photo-thermo semi-hydrogenation of acetylene on Pd_1/TiO_2 single-atom catalyst. *Nat. Commun.* **13**, 2648 (2022).

29. J. Shan, C. Ye, C. Zhu, J. Dong, W. Xu, L. Chen, Y. Jiao, Y. Jiang, L. Song, Y. Zhang, M. Jaroniec, Y. Zhu, Y. Zheng, S.-Z. Qiao, Integrating interactive noble metal single-atom catalysts into transition metal oxide lattices. *J. Am. Chem. Soc.* **144**, 23214–23222 (2022).

30. H. Jin, X. Liu, P. An, C. Tang, H. Yu, Q. Zhang, H.-J. Peng, L. Gu, Y. Zheng, T. Song, K. Davey, U. Paik, J. Dong, S.-Z. Qiao, Dynamic rhenium dopant boosts ruthenium oxide for durable oxygen evolution. *Nat. Commun.* **14**, 354 (2023).

31. P. Liu, Y. Zhao, R. Qin, S. Mo, G. Chen, L. Gu, D. M. Chevrier, P. Zhang, Q. Guo, D. Zang, B. Wu, G. Fu, N. Zheng, Photochemical route for synthesizing atomically dispersed palladium catalysts. *Science* **352**, 797–800 (2016).

32. S. Zhang, Y. Zhao, R. Shi, C. Zhou, G. I. N. Waterhouse, L.-Z. Wu, C.-H. Tung, T. Zhang, Efficient photocatalytic nitrogen fixation over $Cu^{\delta+}$-modified defective ZnAl-layered double hydroxide nanosheets. *Adv. Energy Mater.* **10**, 1901973 (2020).

33. K. Fujiwara, U. Muller, S. E. Pratsinis, Pd subnano-clusters on TiO_2 for solar-light removal of NO. *ACS Catal.* **6**, 1887–1893 (2016).

34. L. Kuai, Z. Chen, S. Liu, E. Kan, N. Yu, Y. Ren, C. Fang, X. Li, Y. Li, B. Geng, Titania supported synergistic palladium single atoms and nanoparticles for room temperature ketone and aldehydes hydrogenation. *Nat. Commun.* **11**, 48 (2020).

35. K. Fujiwara, S. E. Pratsinis, Single Pd atoms on TiO_2 dominate photocatalytic NO_x removal. *Appl Catal B* **226**, 127–134 (2018).

36. W. Zhang, C. Fu, J. Low, D. Duan, J. Ma, W. Jiang, Y. Chen, H. Liu, Z. Qi, R. Long, Y. Yao, X. Li, H. Zhang, Z. Liu, J. Yang, Z. Zou, Y. Xiong, High-performance photocatalytic nonoxidative conversion of methane to ethane and hydrogen by heteroatoms-engineered TiO_2. *Nat. Commun.* **13**, 2806 (2022).

37. L. Kuai, S. Liu, S. Cao, Y. Ren, E. Kan, Y. Zhao, N. Yu, F. Li, X. Li, Z. Wu, X. Wang, B. Geng, Atomically dispersed Pt/metal oxide mesoporous catalysts from synchronous pyrolysis-deposition route for water-gas shift reaction. *Chem. Mater.* **30**, 5534–5538 (2018).

38. L. Luo, L. Fu, H. Liu, Y. Xu, J. Xing, C.-R. Chang, D.-Y. Yang, J. Tang, Synergy of Pd atoms and oxygen vacancies on In_2O_3 for methane conversion under visible light. *Nat. Commun.* **13**, 2930 (2022).

39. L. Liu, A. Corma, Metal catalysts for heterogeneous catalysis: From single atoms to nanoclusters and nanoparticles. *Chem. Rev.* **118**, 4981–5079 (2018).

40. M. G. Walter, E. L. Warren, J. R. McKone, S. W. Boettcher, Q. Mi, E. A. Santori, N. S. Lewis, Solar water splitting cells. *Chem. Rev.* **110**, 6446–6473 (2010).

41. W.-M. Cheng, R. Shang, Y. Fu, Irradiation-induced palladium-catalyzed decarboxylative desaturation enabled by a dual ligand system. *Nat. Commun.* **9**, 5215 (2018).

42. G.-Z. Wang, R. Shang, W.-M. Cheng, Y. Fu, Irradiation-induced Heck reaction of unactivated alkyl halides at room temperature. *J. Am. Chem. Soc.* **139**, 18307–18312 (2017).

43. P. Chuentragool, M. Parasram, Y. Shi, V. Gevorgyan, General, mild, and selective method for desaturation of aliphatic amines. *J. Am. Chem. Soc.* **140**, 2465–2468 (2018).

44. J. Liu, M. Jiao, L. Lu, H. M. Barkholtz, Y. Li, Y. Wang, L. Jiang, Z. Wu, D. Liu, L. Zhuang, C. Ma, J. Zeng, B. Zhang, D. Su, P. Song, W. Xing, W. Xu, Y. Wang, Z. Jiang, G. Sun, High performance platinum single atom electrocatalyst for oxygen reduction reaction. *Nat. Commun.* **8**, 15938 (2017).

45. M. Du, Y. Zhang, S. Kang, X. Guo, Y. Ma, M. Xing, Y. Zhu, Y. Chai, B. Qiu, Trash to treasure: Photoreforming of plastic waste into commodity chemicals and hydrogen over MoS_2-tipped CdS nanorods. *ACS Catal.* **12**, 12823–12832 (2022).

46. X. Jiao, K. Zheng, Q. Chen, X. Li, Y. Li, W. Shao, J. Xu, J. Zhu, Y. Pan, Y. Sun, Y. Xie, Photocatalytic conversion of waste plastics into C_2 fuels under simulated natural environment conditions. *Angew. Chem. Int. Ed.* **59**, 15497–15501 (2020).

47. C. Cassani, G. Bergonzini, C.-J. Wallentin, Photocatalytic decarboxylative reduction of carboxylic acids and its application in asymmetric synthesis. *Org. Lett.* **16**, 4228–4231 (2014).

48. D. W. Manley, J. C. Walton, A clean and selective radical homocoupling employing carboxylic acids with titania photoredox catalysis. *Org. Lett.* **16**, 5394–5397 (2014).

49. J. Guo, Y. Zheng, Z. Hu, C. Zheng, J. Mao, K. Du, M. Jaroniec, S.-Z. Qiao, T. Ling, Direct seawater electrolysis by adjusting the local reaction environment of a catalyst. *Nat. Energy* **8**, 264–272 (2023).

50. D. Li, Y. Zhao, Y. Miao, C. Zhou, L.-P. Zhang, L.-Z. Wu, T. Zhang, Accelerating electron-transfer dynamics by TiO_2-immobilized reversible single-atom copper for enhanced artificial photosynthesis of urea. *Adv. Mater.* **34**, e2207793 (2022).

51. R. Chen, F. Fan, T. Dittrich, C. Li, Imaging photogenerated charge carriers on surfaces and interfaces of photocatalysts with surface photovoltage microscopy. *Chem. Soc. Rev.* **47**, 8238–8262 (2018).

52. D. Gross, I. Mora-Seró, T. Dittrich, A. Belaidi, C. Mauser, A. J. Houtepen, E. D. Como, A. L. Rogach, J. Feldmann, Charge separation in type II tunneling multilayered structures of CdTe and CdSe nanocrystals directly proven by surface photovoltage spectroscopy. *J. Am. Chem. Soc.* **132**, 5981–5983 (2010).

53. J. Ran, H. Zhang, S. Fu, M. Jaroniec, J. Shan, B. Xia, Y. Qu, J. Qu, S. Chen, L. Song, J. M. Cairney, L. Jing, S.-Z. Qiao, $NiPS_3$ ultrathin nanosheets as versatile platform advancing highly active photocatalytic H_2 production. *Nat. Commun.* **13**, 4600 (2022).

54. Y. Sun, W. Chang, H. Ji, C. Chen, W. Ma, J. Zhao, An unexpected fluctuating reactivity for odd and even carbon numbers in the TiO_2-based photocatalytic decarboxylation of C_2-C_6 dicarboxylic acids. *Chemistry* **20**, 1861–1870 (2014).

55. I. Dolamic, T. Bürgi, Photocatalysis of dicarboxylic acids over TiO_2: An in situ ATR-IR study. *J. Catal.* **248**, 268–276 (2007).

56. S. Kang, B. Xing, Adsorption of dicarboxylic acids by clay minerals as examined by in situ ATR-FTIR and ex situ DRIFT. *Langmuir* **23**, 7024–7031 (2007).

57. L. Chen, Y. Li, X. Zhang, Q. Zhang, T. Wang, L. Ma, Mechanistic insights into the effects of support on the reaction pathway for aqueous-phase hydrogenation of carboxylic acid over the supported Ru catalysts. *Appl. Catal. A. Gen.* **478**, 117–128 (2014).

58. I. Dolamic, T. Bürgi, Photoassisted decomposition of malonic acid on TiO_2 studied by in situ attenuated total reflection infrared spectroscopy. *J. Phys. Chem. B* **110**, 14898–14904 (2006).

59. S. Zhang, Y. Zhao, Y. Miao, Y. Xu, J. Ran, Z. Wang, Y. Weng, T. Zhang, Understanding aerobic nitrogen photooxidation on titania through in situ time-resolved spectroscopy. *Angew. Chem. Int. Ed.* **61**, e202211469 (2022).

60. C. Wang, X. Li, Y. Ren, H. Jiao, F. R. Wang, J. Tang, Synergy of Ag and AgBr in a pressurized flow reactor for selective photocatalytic oxidative coupling of methane. *ACS Catal.* **13**, 3768–3774 (2023).

61. M.-Y. Gao, H. Bai, X. Cui, S. Liu, S. Ling, T. Kong, B. Bai, C. Hu, Y. Dai, Y. Zhao, L. Zhang, J. Zhang, Y. Xiong, Precisely tailoring heterometallic polyoxotitanium clusters for the efficient and selective photocatalytic oxidation of hydrocarbons. *Angew. Chem. Int. Ed.* **61**, e202215540 (2022).

62. Y. Chen, C. Zou, M. Mastalerz, S. Hu, C. Gasaway, X. Tao, Applications of micro-Fourier transform infrared spectroscopy (FTIR) in the geological sciences—A review. *Int. J. Mol. Sci.* **16**, 30223–30250 (2015).

63. C. M. Pichler, S. Bhattacharjee, E. Lam, L. Su, A. Collauto, M. M. Roessler, S. J. Cobb, V. M. Badiani, M. Rahaman, E. Reisner, Bio-electrocatalytic conversion of food waste to ethylene via succinic acid as the central intermediate. *ACS Catal.* **12**, 13360–13371 (2022).

64. L. M. Betts, F. Dappozze, C. Guillard, Understanding the photocatalytic degradation by P25 TiO_2 of acetic acid and propionic acid in the pursuit of alkane production. *Appl. Catal. A. Gen.* **554**, 35–43 (2018).

65. Y. Nosaka, A. Y. Nosaka, Generation and detection of reactive oxygen species in photocatalysis. *Chem. Rev.* **117**, 11302–11336 (2017).

66. S. Zhang, H. Li, L. Wang, J. Liu, G. Liang, K. Davey, J. Ran, S.-Z. Qiao, Boosted photoreforming of plastic waste via defect-rich $NiPS_3$ nanosheets. *J. Am. Chem. Soc.* **145**, 6410–6419 (2023).

67. D. Ma, S. Zhai, Y. Wang, A. Liu, C. Chen, TiO_2 photocatalysis for transfer hydrogenation. *Molecules* **24**, 330 (2019).

68. J. M. Ferreira, Jr., G. F. Trindade, R. Tshulu, J. F. Watts, M. A. Baker, Dicarboxylic acids analysed by x-ray photoelectron spectroscopy, Part II—Butanedioic acid anhydrous. *Surf. Sci. Spectra* **24**, 011102 (2017).

69. B.-H. Lee, S. Park, M. Kim, A. K. Sinha, S. C. Lee, E. Jung, W. J. Chang, K.-S. Lee, J. H. Kim, S.-P. Cho, H. Kim, K. T. Nam, T. Hyeon, Reversible and cooperative photoactivation of single-atom Cu/TiO_2 photocatalysts. *Nat. Mater.* **18**, 620–626 (2019).

70. X. Sun, J. Chen, T. Ritter, Catalytic dehydrogenative decarboxyolefination of carboxylic acids. *Nat. Chem.* **10**, 1229–1233 (2018).

71. C. Kang, L. Jing, T. Guo, H. Cui, J. Zhou, H. Fu, Mesoporous SiO_2-modified nanocrystalline TiO_2 with high anatase thermal stability and large surface area as efficient photocatalyst. *J. Phys. Chem. C* **113**, 1006–1013 (2009).

72. R. Bagri, P. T. Williams, Catalytic pyrolysis of polyethylene. *J. Anal. Appl. Pyrolysis* **63**, 29–41 (2002).

73. M. Artetxe, G. Lopez, M. Amutio, G. Elordi, J. Bilbao, M. Olazar, Cracking of high density polyethylene pyrolysis waxes on HZSM-5 catalysts of different acidity. *Ind. Eng. Chem. Res.* **52**, 10637–10645 (2013).

74. F. Ateş, N. Miskolczi, N. Borsodi, Comparision of real waste (MSW and MPW) pyrolysis in batch reactor over different catalysts. Part I: Product yields, gas and pyrolysis oil properties. *Bioresour. Technol.* **133**, 443–454 (2013).

75. N. Lee, J. Joo, K.-Y. A. Lin, J. Lee, Waste-to-fuels: Pyrolysis of low-density polyethylene waste in the presence of H-ZSM-11. *Polymers* **13**, 1198 (2021).

76. M. Kusenberg, M. Roosen, A. Zayoud, M. R. Djokic, H. D. Thi, S. D. Meester, K. Ragaert, U. Kresovic, K. M. V. Geem, Assessing the feasibility of chemical recycling via steam cracking of untreated plastic waste pyrolysis oils: Feedstock impurities, product yields and coke formation. *Waste Manag.* **141**, 104–114 (2022).

77. I. I. Ahmed, N. Nipattummakul, A. K. Gupta, Characteristics of syngas from co-gasification of polyethylene and woodchips. *Appl. Energy* **88**, 165–174 (2011).

78. A. Eschenbacher, F. Goodarzi, R. J. Varghese, K. Enemark-Rasmussen, S. Kegnæs, M. S. Abbas-Abadi, K. M. V. Geem, Boron-modified mesoporous ZSM-5 for the conversion of pyrolysis vapors from LDPE and mixed polyolefins: Maximizing the C_2–C_4 olefin yield with minimal carbon footprint. *ACS Sustainable Chem. Eng.* **9**, 14618–14630 (2021).

79. W. Kaminsky, B. Schlesselmann, C. Simon, Olefins from polyolefins and mixed plastics by pyrolysis. *J. Anal. Appl. Pyrolysis* **32**, 19–27 (1995).

80. E. Bäckström, K. Odelius, M. Hakkarainen, Trash to treasure: Microwave-assisted conversion of polyethylene to functional chemicals. *Ind. Eng. Chem. Res.* **56**, 14814–14821 (2017).

81. T. Uekert, H. Kasap, E. Reisner, Photoreforming of nonrecyclable plastic waste over a carbon nitride/nickel phosphide catalyst. *J. Am. Soc. Chem.* **141**, 15201–15210 (2019).

82. J. Xu, X. Jiao, K. Zheng, W. Shao, S. Zhu, X. Li, J. Zhu, Y. Pan, Y. Sun, Y. Xie, Plastics-to-syngas photocatalysed by Co-Ga_2O_3 nanosheets. *Natl. Sci. Rev.* **9**, nwac011 2022.

83. Z. Huang, M. Shanmugam, Z. Liu, A. Brookfield, E. L. Bennett, R. Guan, D. E. Vega Herrera, J. A. Lopez-Sanchez, A. G. Slater, E. J. L. Mclnnes, X. Qi, J. Xiao, Chemical recycling of polystyrene to valuable chemicals via selective acid-catalyzed aerobic oxidation under visible light. *J. Am. Soc. Chem.* **144**, 6532–6542 (2022).

84. J. Qin, Y. Dou, J. Zhou, V. M. Candelario, H. R. Andersen, C. Helix-Nielsen, W. Zhang, Photocatalytic valorization of plastic waste over zinc oxide encapsulated in a metal-organic framework. *Adv. Funct. Mater.* **33**, 2214839 (2023).

85. J. Ye, Y. Chen, C. Gao, C. Wang, A. Hu, G. Dong, Z. Chen, S. Zhou, Y. Xiong, Sustainable conversion of microplastics to methane with ultrahigh selectivity by a biotic-abiotic hybrid photocatalytic system. *Angew. Chem. Int. Ed.* **61**, e202213244 (2022).

86. R. Cao, M.-Q. Zhang, C. Hu, D. Xiao, M. Wang, D. Ma, Catalytic oxidation of polystyrene to aromatic oxygenates over a graphitic carbon nitride catalyst. *Nat. Commun.* **13**, 4809 (2022).

87. Y. Liu, X. Wang, Q. Li, T. Yan, X. Lou, C. Zhang, M. Cao, L. Zhang, T.-K. Sham, Q. Zhang, L. He, J. Chen, Photothermal catalytic polyester upcycling over cobalt single-site catalyst. *Adv. Funct. Mater.* **33**, 2210283 (2023).

88. S. Bhattacharjee, V. Andrei, C. Pornrungroj, M. Rahaman, C. M. Pichler, E. Reisner, Reforming of soluble biomass and plastic derived waste using a bias-free $Cu_{30}Pd_{70}$|perovskite|Pt photoelectrochemical device. *Adv. Funct. Mater.* **32**, 2109313 (2021).

89. C.-Y. Lin, S.-C. Huang, Y.-G. Lin, L.-C. Hsu, C.-T. Yi, Electrosynthesized Ni-P nanospheres with high activity and selectivity towards photoelectrochemical plastics reforming. *Appl Catal B* **296**, 120351 (2021).